Title
Repeated Exposure to Multiple Concurrent Stresses Induce Circuit Specific Loss of Inputs to the Posterior Parietal Cortex

Journal
Journal of Neuroscience, 40(9)

ISSN
0270-6474

Authors
Libovner, Yaaqov
Fariborzi, Mona
Tabba, Daim
et al.

Publication Date
2020-02-26

DOI
10.1523/jneurosci.1838-19.2020

Peer reviewed

Systems/Circuits

Repeated Exposure to Multiple Concurrent Stresses Induce Circuit Specific Loss of Inputs to the Posterior Parietal Cortex

Yaaqov Libovner, Mona Fariborzi, Daim Tabba, Ali Ozgur, Tamara Jafar, and Gyorgy Lur
Department of Neurobiology and Behavior University of California, Irvine, Irvine, California 92697

Severe loss of excitatory synapses in key brain regions is thought to be one of the major mechanisms underlying stress-induced cognitive impairment. To date, however, the identity of the affected circuits remains elusive. Here we examined the effect of exposure to repeated multiple concurrent stressors (RMS) on the connectivity of the posterior parietal cortex (PPC) in adolescent male mice. We found that RMS led to layer-specific elimination of excitatory synapses with the most pronounced loss observed in deeper cortical layers. Quantitative analysis of cortical projections to the PPC revealed a significant loss of sensory and retrosplenial inputs to the PPC while contralateral and frontal projections were preserved. These results were confirmed by decreased synaptic strength from sensory, but not from contralateral, projections in stress-exposed animals. Functionally, RMS disrupted visuospatial working memory performance, implicating disrupted higher-order visual processing. These effects were not observed in mice subjected to restraint-only stress for an identical period of time. The PPC is considered to be a cortical hub for multisensory integration, working memory, and perceptual decision-making. Our data suggest that sensory information streams targeting the PPC may be impacted by recurring stress, likely contributing to stress-induced cognitive impairment.

Key words: **chronic stress; multimodal stress; posterior parietal cortex; retrograde tracing; synapse loss; visuospatial working memory**

Significance Statement

Repeated exposure to stress profoundly impairs cognitive functions like memory, attention, or decision-making. There is emerging evidence that stress not only impacts high-order regions of the brain, but may affect earlier stages of cognitive processing. Our work focuses on the posterior parietal cortex, a brain region supporting short-term memory, multisensory integration, and decision-making. We show evidence that repeated stress specifically damages sensory inputs to this region. This disruption of synaptic connectivity is linked to working memory impairment and is specific to repeated exposure to multiple stressors. Altogether, our data provide a potential alternative explanation to ailments previously attributed to downstream, cognitive brain structures.

Introduction

Repeated exposure to stress impedes executive functions, including navigation and working memory (Conrad et al., 1996; Luethi et al., 2008). Such adversities in early life have especially drastic effects on the nervous system (Lupien et al., 2009). While the detrimental nature of parental and neonatal stress has long been appreciated, more recent experiments highlight increased vulnerability to stress during adolescence (Eiland and Romeo, 2013). Chronic stress in adolescent rodents resulted in an increased activation of the hypothalamic-pituitary-adrenal axis (Romeo et al., 2006), dendritic atrophy (Eiland et al., 2012), and exacerbated behavioral deficits (Avital and Richter-Levin, 2005) compared with the same stress exposure in adults. These findings correlate with an increased susceptibility to psychological disorders observed in adolescent humans (Gomes and Grace, 2017).

The behavioral effects of chronic stress have long been attributed to damage in brain regions linked to the highest levels of cognitive function—the hippocampus and the prefrontal cortex (PFC). This notion is based on evidence that stress impairs performance in spatial and memory tasks (Luine et al., 1994; Mizoguchi et al., 2000), induces synapse loss in both structures (Sousa et al., 2000; Radley et al., 2006), and leads to altered functional

Received July 30, 2019; revised Jan. 6, 2020; accepted Jan. 9, 2020.
Author contributions: Y.L., M.F., D.T., A.O., T.J., and G.L. performed research; G.L. designed research; Y.L., M.F., D.T., A.O., T.J., and G.L. analyzed data; G.L. wrote the paper.
This work was funded by University of California, Irvine, setup funds (G.L.) and the Whitehall Foundation 3-Year Research Grant 2018-12-09 (G.L.).
The authors declare no competing financial interests.
Correspondence should be addressed to Gyorgy Lur at glur@uci.edu.
https://doi.org/10.1523/JNEUROSCI.1838-19.2020

connectivity in human subjects (Liston et al., 2009; Soares et al., 2012). Although data from other brain areas are scarce, in rodents, chronic stress was shown to impair texture discrimination and cause dendritic spine loss in the somatosensory cortex (Chen et al., 2018) and to induce mild atrophy of the right visual cortex measured by voxel-based morphometry (Yoshii et al., 2017). Furthermore, a 10-fold increase in c-Fos $^+$ cells was detected in parietal, visual, retrosplenial, and auditory cortices of stressed rats, an increase comparable to or exceeding labeling in regions traditionally associated with stress (Lkhagvasuren et al., 2014). Stress-induced disruption of auditory and visual processing was also reported in humans (Shackman et al., 2011; Dagnino-Subiabre, 2013). These findings motivate our hypothesis that the effects of stress are not limited to brain regions associated with the highest levels of cognitive function but extend to earlier stages of processing.

The posterior parietal cortex (PPC) is an association area (Kolb and Walkey, 1987; Reep et al., 1994) that has been linked to multisensory integration, navigation, working memory, and decision-making in rodents, primates, and humans (McNaughton et al., 1994; Andersen and Cui, 2009; Noudoost et al., 2010; Brodt et al., 2016; Mohan et al., 2018). Its role as a cognitive hub hinges on a high degree of connectivity. Indeed, the PPC receives synaptic input from visual, auditory, and somatosensory cortices (Mazzoni et al., 1996; Andersen et al., 1997; Olcese et al., 2013; Mohan et al., 2018; Zhong et al., 2019) as well as top-down afferents from frontal and retrosplenial cortices (Corwin and Reep, 1998; Wilber et al., 2015). Although this suggests that the PPC may be vulnerable to insult that damages synaptic connections, data on how stress affects the PPC is scarce. Functional imaging studies revealed altered metabolism and connectivity of the parietal lobe in subjects exposed to trauma or abuse (Bremner et al., 1999a; Lanius et al., 2002; Liston et al., 2009; Hart et al., 2017). Yet, how stress affects synaptic connections of the PPC is currently unknown.

Therefore, we examined the effects of repeated stress exposure on the input network of the PPC in adolescent mice. Given the capacity of the PPC to process information from several sensory modalities, we used a multimodal stress paradigm combining physical, visual, and auditory stressors. We found that repeated stress activated the PPC and induced a marked loss of excitatory synapses. Anatomical and electrophysiological measurements suggested that projections from sensory and retrosplenial cortices were more susceptible to stress than inputs from the contralateral PPC (cPPC) or the anterior cingulate cortex (ACC). In agreement with these results, stress disrupted visuospatial working memory. Overall, our findings indicate that chronic stress alters cortical connectivity in a circuit-specific manner.

Materials and Methods

Animals. Animals were group housed in a quiet, uncrowded facility on a 12 h light/dark cycle, with *ad libitum* access to food and water. For all procedures, male C57BL/6 mice were either purchased from Charles River or bred in house. At postnatal day 30 (P30) to P35, male age-matched mice were randomly divided into the following two groups: control or stressed. Experiments were performed in accordance with the NIH guidelines on laboratory animal welfare and were approved by the University of California Irvine Institutional Animal Care and Use Committee.

Stress paradigms. At age P30 to P35, male mice were randomly assigned to experimental groups: repeated multiple concurrent stressors (RMS) or stress-free control. For RMS, animals were placed in a well vented restrainer fashioned from 50 ml conical tubes, and five to eight mice were then placed in a clean cage. A high-frequency speaker was placed in the cage to deliver loud noise stimulus. The noise was generated by an Arduino Uno driving an amplifier and consisted of 0.5–1-s-long beeps randomly selected from a frequency range of 15–30 kHz at 0.5–3 s random intervals. The cage was placed on top of a laboratory rocker under a bright light. Animals were rocked for 1 h/d for 10 consecutive days. A subset of control and stressed mice were weighed every day before the onset of RMS. On day 10, animals were subjected to behavioral studies or killed for histological or electrophysiology testing.

Restraint-only stress (ROS) consisted of physical confinement to the above-described retainer for 1 h/d for 10 d. No more than two restrained animals were placed in a clean cage and kept in darkness for the stress duration.

Visual exposure (VIS) consisted of the exact same illumination as the RMS paradigm but without any other stressors. Animals were exposed to the light for 1 h/d for 10 d.

Immunohistochemistry. For immune staining, pairs of age-matched control and stressed mice were transcardially perfused with PBS followed by 4% paraformaldehyde (PFA) dissolved in Sorenson's buffer and post-fixed for 5 h in 4% PFA. After 5 h, the solution was replaced with Sorenson's buffer, and 50 μm coronal slices were prepared from the posterior parietal region on a vibrating microtome (Compresstome 300z). Slices were washed in Sorenson's buffer and nonspecific staining was blocked for 1 h at room temperature (RT) with 10% normal goat serum (NGS), 1%h bovine serum albumin (BSA) and 0.1% Triton X-100 dissolved in Sorenson's buffer. After blocking, slices were transferred to a staining solution with 5% NGS, 1% BSA, and anti-postsynaptic density-95 (PSD-95) monoclonal antibody (7E3–1B8, Thermo Fisher Scientific) at 1:2000 dilution or anti-c-Fos (Synaptic Systems) at 1:5000 dilution in Sorenson's buffer for overnight staining at 4°C on a laboratory shaker. Stained slices were washed four times in Sorenson's buffer and transferred into a secondary antibody solution containing anti-mouse secondary antibody conjugated to Alexa Fluor 555 (1:500) and the fluorescent Nissl stain Neurotrace 430 (1:100; Thermo Fisher Scientific) for 2 h. Following four washes with Sorenson's buffer, slices were mounted on microscope slides with Prolong Diamond anti-fade reagent and covered with a no. 1 thickness cover glass. All staining batches contained age-matched control and stressed brains to assure even staining between conditions.

Retrograde labeling. To label neurons projecting to the PPC both control and stressed mice were injected with either 150 nl red latex microbeads (Lumafluor) or with 150 nl of Alexa Fluor 555 dye-conjugated choleratoxin B subunit (CTB; Thermo Fisher Scientific) on day 4 of the stress protocol. Transcranial injections were targeted to the right PPC, as follows: anteroposterior (AP), 2.1 mm; mediolateral (ML), 1.7 mm; dorsoventral (DV), 0.45 mm from the bregma, using a pulled glass pipette (Sutter Instruments) in a microinjector pump (UMP3, World Precision Instruments) attached to a stereotaxic frame (Kopf Instruments). After completion of the stress protocol, animals were transcardially perfused with 4% PFA in Sorenson's buffer. The extracted brains were postfixed overnight in 4% PFA at 4°C then PFA was replaced with Sorenson's buffer. Fifty micrometer coronal sections were prepared using a vibrating blade microtome (Compresstome), washed in Sorenson's buffer and stained for 2 h with Neurotrace 430 (1:100) as per manufacturer instructions. Stained slices were mounted on microscope slides with Prolong Diamond anti-fade reagent.

Confocal microscopy. PSD-95 staining was visualized on an LSM 700 Confocal Microscope (Zeiss) in the University of California, Irvine, Optical Biology Core using a 63× oil-immersion objective. Hippocampal images were taken as 5 × 5 tiles at 1× optical zoom (0.2 μm pixel size) to include all layers of the hippocampus. PPC images were 3 × 10 tiles at 1× optical zoom to include the entire cortical column. Images were taken 10 μm from the slice surface to ensure identical antibody penetration between slices. The PPC was imaged at 1500–1700 μm from the midline. Neurotrace 430 and Alexa Fluor 555 were excited at 405 and 555 nm, respectively. Fluorescence emissions were separated using a 500 nm beam splitter and filtered with 490 nm short-pass and 560 nm long-pass filters.

Retrograde labels (retrobeads and CTB) were imaged on the same LSM 700 confocal microscope through a 40× oil-immersion objective. Cortical regions of interest included the ACC, the cPPC, the somatosen-

sory barrel cortex (S1), the auditory cortex (A1), and the primary visual cortex (V1). At each region 5 × 5 tiles at 1× optical zoom (0.31 μm pixel size) captured an 800.22 × 800.22 μm square of tissue at two focal depths with minimum 15 μm separation between optical sections. Excitation and emission filters were set as described above.

Wide-field imaging. To illustrate the cortical regions, we used to assess long-range connectivity of the PPC, we used wide-field imaging of brain slices from the ACC, the cPPC, the S1, the A1, and the V1. Slices containing retrogradely labeled projection neurons in the above brain regions were stained with NeuroTrace 430. Epifluorescent images of whole-brain slices were captured on a fully motorized Olympus BX63 microscope using a 10× objective. Fluorescence was excited using a mercury bulb light source filtered at 405 and 550 nm, and emissions were collected with DAPI and TexasRed filter sets. Tiling and assembly were accomplished via Cell Sense software. Acquired images were subject to linear adjustments of contrast and brightness in ImageJ (NIH).

Image quantification. Synaptic density and projection cell numbers were automatically quantified in CellProfiler (Lamprecht et al., 2007; McQuin et al., 2018). To avoid experimenter biases, all conditions (control and stressed) were loaded simultaneously, and the analysis was run on this combined batch of images. To count PSD-95 puncta in the hippocampus and PPC, full sized confocal images were loaded into CellProfiler and automatically assigned into their respective groups (animal, treatment group, brain region, section) based on metadata extracted from the image files. PSD-95 puncta were detected in the red channel via an object identification algorithm with object size ranging from 2 to 8 pixels and adaptive intensity thresholding with a window of 10 pixels. Somata were identified in the Neurotrace channel with object size ranging from 30 to 120 pixels. Synaptic density was then expressed as the number of puncta per 100 μm^2 of brain tissue. For synapse density in distinct cortical layers, 100 μm^2 subsections were randomly cropped from visually identified cortical layers and analyzed using the same pipeline.

Retrogradely labeled projection neurons and c-Fos$^+$ cells were counted using object recognition pipelines in CellProfiler. In the red channel, red retrobeads were defined as objects ranging from 2 to 15 pixels, while CTB$^+$ cell bodies were 30–120 pixels. Total neuron count was established using the Neurotrace channel as above. Cells were counted as retrograde/c-fos$^+$ if they had more than five retrobeads or at least 1 CTB/c-Fos-labeled particle within a Neurotrace-labeled soma and expressed as a percentage of all cell bodies in the image. Laminar distribution of c-Fos-labeled neurons was examined using a histogram of the number of c-Fos$^+$ neurons collected into 25 μm spatial bins from the pial surface. The number of cells in each spatial bin was the average of all RMS mice.

Optogenetics expression and activation. To stimulate long-range inputs to the PPC, we expressed the channelrhodopsin variant Chronos (Klapoetke et al., 2014) in either A1 or in cPPC. The day before we started the stress paradigm, P30 to P35 age-matched control and to-be-stressed mice were injected with 200 nl of adeno-associated virus (AAV) carrying Chronos-EYFP (enhanced yellow fluorescent protein) fusion protein under the human synapsin promoter (AAV2.9-hSyn-Chronos-EYFP). The virus was produced by the Penn Vector Core (currently Addgene). We stereotaxically targeted the auditory cortex (anteroposterior, 2.8 mm; mediolateral, 4.1 mm; dorsoventral, 0.8 mm from the bregma) or the left PPC (anteroposterior, 2.1 mm; mediolateral, 1.7 mm; dorsoventral, 0.45 mm from the bregma)s. The same injection apparatus was used as described above.

Acute slices from the right PPC were prepared on the 10th day of RMS, as described below. Control and stressed mice were recorded in pairs on the same day. We activated Chronos$^+$ fibers using 50-μs-long pulses from a 460 nm LED (optical beam combiner, Sutter Instrument) through the microscope objective (60×; Olympus).

Electrophysiology. To measure the intrinsic properties of PPC neurons and the strength of long-range connections, we made whole-cell current-clamp recordings. To avoid possible time-sensitive changes in physiological properties, we recorded from both control and stressed mice on the same day. Under isoflurane anesthesia, mice were transcardially perfused with cutting solution containing the following (in mM): 110 choline, 25 NaHCO3, 1.25 NaH_2PO_4, 3 KCl, 7 MgCl2, 0.5 CaCl2, 10 glucose, 11.6 sodium ascorbate, and 3.1 sodium pyruvate, bubbled with 95% O_2 and 5% CO_2. The 300-μm-thick slices containing the PPC were prepared on a vibrating blade microtome (Campden smz 7000–2, Lafayette Instruments) and maintained in the cutting solution for an additional 15 min at 32°C (Ting et al., 2014). After incubation, slices were transferred to artificial CSF (ACSF) containing the following (in mM): 126 NaCl, 26 NaHCO3, 1.25 NaH_2PO_4, 3 KCl, 1 MgCl2, 2 CaCl2, and 10 glucose, bubbled with 95% O_2 and 5% CO_2 in a holding chamber at RT and maintained for 20–30 min before use.

All experiments were conducted in a submersion type recording chamber mounted on an Olympus BX51-WI Microscope. We limited recordings to RT (24–25°C) to better maintain neuron health during long (40+ minutes) recording sessions. Whole-cell patch-clamp recordings were obtained from superficial layer 5 pyramidal cells (250–400 μm from the pia surface) identified with video-infrared/differential interference contrast. For all recordings, glass electrodes (2–4 MΩ) were filled with internal solution containing the following (in mM): 135 KMeSO3, 10 HEPES, 4 MgCl2, 4 Na2ATP, 0.4 NaGTP, and 10 sodium creatine phosphate, and adjusted to pH 7.3 with KOH. Series resistance was 10–22 MΩ and bridge compensated. Electrophysiological recordings were made using a MultiClamp 700B Amplifier (Molecular Devices), filtered at 4 kHz, and digitized at 10 kHz. Data was acquired using National Instruments DAQ boards and Wavesurfer software written in Matlab (Howard Hughes Medocal Institute Janelia Research Campus). Offline analysis was performed using custom routines in Matlab and python. To measure the intrinsic properties of cells, we injected 13 current pulses equally spaced from −300 to +300 pA. Action potential peaks were automatically identified with a peak finder algorithm, and action potential number, height, timing, and width were saved. Resting membrane potential was measured during the first 900 ms of each recording and expressed as an average of 13 trials. Input resistance was measured at the membrane response to −200 pA and at +50 pA current injections.

To estimate connection strength between brain regions in age-matched control and stressed animals, we expressed the excitatory opsin Chronos in the right A1 or in the left (contralateral to the recording) PPC. After the end of the stress paradigm, we prepared acute slices from the right PPC and made whole-cell current-clamp recordings from layer 5 pyramidal cells ~1500 μm from the midline. We stimulated Chronos-expressing long-range axons with increasingly strong 460 nm light pulses until the cell started firing action potentials or until we maxed out LED power. Following current-clamp recordings, we switched to voltage clamp and measured light-evoked excitatory currents at −70 mV holding potential and inhibitory currents at 0 mV holding potential in response to five light pulses with increasing intensity. It is to be noted that voltage-clamp recordings were made using K^+-based internal solutions, restricting space clamp and thus biasing recorded IPSCs to synapses close to the soma.

Behavior. To measure spontaneous alternation, we used a homemade Y-maze that consisted of three 350-mm-long and 75-mm-wide arms fabricated from 3-mm-thick opaque-gray acrylic sheets positioned at 120° angles from each other. The maze was built on a 6-mm-thick, white acrylic base. We positioned a wide angle (100°) webcam (generic brand from amazon.com) ~50 cm above the maze to record mouse behavior. The entire maze was enclosed in a light box constructed from "quick frame" (80/20) and diffuser fabric to block out any distractions. Large geometrical shapes were displayed on the walls of the light box, outside of the maze but were positioned at easily visible angles to serve as visual cues. All animals were exposed to the Y-maze for two identical 8 min sessions: first, for a habituation session before stress exposure; and second approximately an hour after the end of the last stress session. Control and stressed animals were placed into a randomly selected arm of the maze, and their behavior was captured on video at 30 frames/s for 6 min. The maze was cleaned with 70% ethyl alcohol between each mouse. Video footage was analyzed using batch processing in Camlytics software and spontaneous alternations were calculated as follows: spontaneous alternation (%) = (number of spontaneous alternations/total number of

arm entries −2) * 100 as in the study by Miedel et al. (2017) using a custom script written in python.

PPC cannula implants and muscimol infusion. For inactivation experiments, we implanted seven mice with bilateral guide cannulas (26G, Plastics One) over the PPC [coordinates (in mm): AP, 2.1 mm; ML, 1.7 mm from the bregma] using dental cement. Mice were allowed to recover for a week. On test day 1, animals were randomly assigned to vehicle (saline) or muscimol groups. We injected 250 nl of $GABA_A$ agonist, muscimol (5 μM), or saline (vehicle control) into the PPC through the guide cannula. We measured spontaneous alternation in the Y-maze 30–45 min after the injection. Two days later, groups were switched, and previously muscimol injected mice got saline while the rest of the mice received muscimol injections. Animals then reran the Y-maze. Comparisons were made between saline control and muscimol conditions within each mouse.

Tetanus toxin expression. To specifically inactivate visual inputs to the PPC, we used a dual-virus strategy. To target neurons projecting to the PPC, mice received bilateral injections of the retrograde AAV-expressing Cre-recombinase (rgAAV-hSyn-Cre-WPRE-hGH, a gift from Dr. James M. Wilson, Perelman School of Medicine at the University of Pennsylvania, produced by plasmid #105553, Addgene) in the PPC (AP, 2.1 mm; ML, 1.7 mm; DV, 0.45 mm from bregma). Subsequently, we bilaterally injected the Cre-dependent tetanus neurotoxin (AAV.DJ-CMV-DIO-eGFP-2A-TeNT, purchased via the Stanford viral core; Xu et al., 2012; Xu and Südhof, 2013; Shang et al., 2018) into the V1 (coordinates: AP, 3.2 mm; ML, 2.3 mm; DV, 0.45 mm from bregma). Age-matched control animals received bilateral retrograde AAV-Cre injection into the PPC and AAV-hSyn-DIO-EGFP into V1. We allowed for 3–4 weeks for expression then measured spontaneous alternation in the Y-maze.

Experimental design and statistical analysis. All histology and physiology data collection were performed in parallel in age-matched control and stressed animals with the experimenter blinded to the condition of the animal. Mouse weights were compared using two-way ANOVA. In all histology experiments, we imaged three to four brain slices per animal for every region of interest. Puncta or cell counts from these slices were then averaged and a single value per animal was used for statistical comparisons; thus, the df (n numbers) for every experiment are individual animals. Where appropriate, one-way ANOVA was used with Bonferroni's *post hoc* test for multiple comparison in Prism 5. Student's t test was only used where only two variables were compared.

In current-clamp electrophysiology experiments, the EPSP response of each cell to increasing stimulus strength was fitted with the following exponential association function: $Y = Y0 + (\text{plateau} - Y0) * (1 - \exp(-K * x))$. In voltage-clamp recordings, EPSCs were fitted with an exponential decay: $Y = (Y0 - \text{plateau}) * \exp(-K * x) + \text{plateau}$, while IPSCs were fitted with the above exponential association. Up to three cells were recorded per mouse. To account for the nested design of our experiment, fit coefficients [plateau and the exponent (K)] from all cells recorded from an animal were averaged, and the mean coefficient value was used for statistical comparison, thus each mouse represented a single observation. The average fits in Figures 4 and 5 are generated from the mean coefficients of all the animals in that particular group. Coefficients were compared within groups using Student's t test.

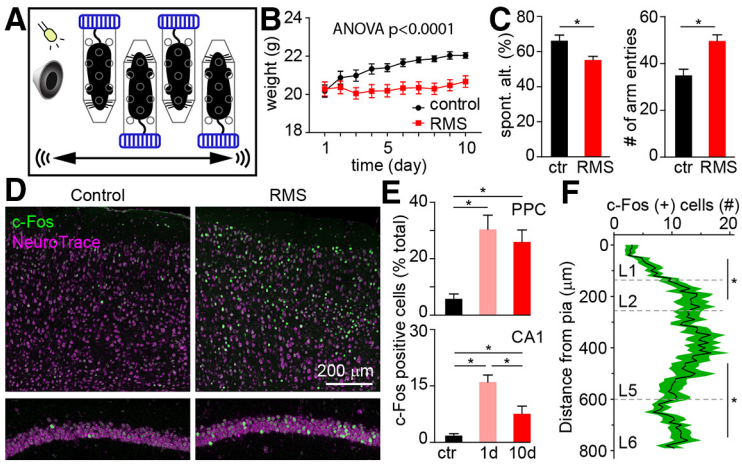

Figure 1. Repeated exposure to multiple concurrent stressors impairs spatial working memory and activates the PPC. ***A***, Schematic of the RMS paradigm. ***B***, Weight change of control (black) and stressed mice (red) during the 10 d exposure to RMS. Data points indicate the mean weight (±SEM) of mice on each day. ***C***, Bar graphs indicate the mean (±SEM) spontaneous alternation rate (left) and the number of arm entries (right) in control (black) and RMS (red) mice. ***D***, Example confocal images of c-Fos labeling (green) in PPC (top row) and CA1 (bottom row) from control animals and mice exposed to RMS. ***E***, Bar graphs represent the mean (±SEM) proportion of c-Fos-labeled neurons in the PPC (top) and the hippocampus (bottom) in control mice (black) and in mice exposed to RMS for 1 d (salmon) or for 10 d (red). ***F***, Histogram representing the distribution of c-Fos $^+$ neurons in the PPC. Mean number of c-Fos $^+$ cells (solid black line) ± SEM (green shading), gray dashed lines mark approximate layers in the PPC. *$p < 0.05$, one-way ANOVA with Bonferroni's multiple-comparison test.

Results

Repeated, multiple concurrent stressors disrupt PPC function

To study the effect of repeated exposure to multiple concurrent stressors (RMS), we adopted and modified a stress paradigm that has previously been shown to affect hippocampal learning and memory in mice via the elimination of mature synapses specifically from the dorsal hippocampus (Chen et al., 2010; Maras et al., 2014). Mice were subjected to a variety of simultaneous stressors including physical stress (restraint and jostling), bright light, and unpredictable noise (Fig. 1*A*) for 1 h/d over a 10 d period. For the duration of the experiment, age-matched control animals remained in their home cages. Over the course of the 10 d, control animals gained weight at the predicted rate while stressed animals failed to gain weight despite *ad libitum* access to food and water (Fig. 1*B*; $p = 0.0082$; RMS exposure explaining 18.71% of the total variance, $n = 12$ control vs $n = 16$ RMS, two-way ANOVA).

In rodents, numerous stress paradigms have been shown to impair navigation and working memory performance (Luine et al., 1994; Conrad et al., 1996; Mizoguchi et al., 2000). To test whether subjecting mice to RMS has similar behavioral effects, we measured the rate of spontaneous alternations between three arms of a Y-maze in age-matched control and stressed mice. This paradigm has been widely used to assess spatial working memory in mice and rats (Conrad et al., 1996; Miedel et al., 2017). We found that RMS reduced spontaneous alternation by 18% ($p = 0.001$, $n = 18$ control and $n = 19$ RMS mice, Student's t test; Fig. 1*C*). This is despite a marked increase in the number of arm entries performed by stressed animals ($p = 0.0001$, $n = 18$ control and $n = 19$ RMS mice, Student's t test; Fig. 1*C*), suggesting that reduced spontaneous alternation was not due to altered locomotion or motivation.

There is mounting evidence that, in concert with the hippocampal formation and the entorhinal cortex, the PPC plays a key role in navigation tasks (Thomas and Weir, 1975; Spangler et al., 1994; Rogers and Kesner, 2006). Specifically, the PPC has been linked to spatial working memory (Save and Poucet, 2000), an attribute frequently measured by the spontaneous alternation rate in the Y-maze. However, the PPC is not a brain region typically associated with stress response. To test whether the PPC is affected by RMS, we quantified the expression of c-Fos, an immediate early gene that is a frequently used indicator of stress-

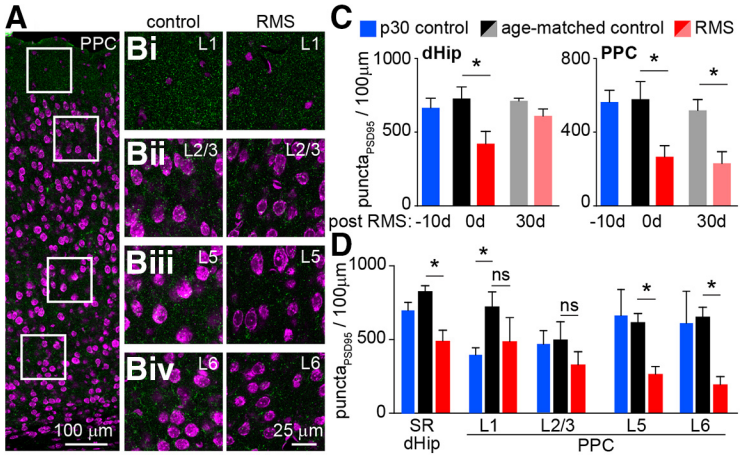

Figure 2. Repeated, multimodal stress causes excitatory synapse loss in the PPC. ***A***, Example confocal image of PSD-95 (green) and NeuroTrace (magenta)-stained PPC section. ***Bi–Biv***, Representative crops for layer 1 (***Bi***), layer 2/3 (***Bii***), layer 5 (***Biii***), and layer 6 (***Biv***) of PPC. ***C***, Bar graphs represent the mean (±SEM) PSD-95 puncta densities in the dorsal hippocampus (dHipp, left), or in the PPC (right). Puncta were quantified at the starting time point in P30 control mice (blue), immediately after the 10 d RMS in P40 control (black) and stressed (red) animals or following a 30 d rest period in P70 control (gray) and stressed (salmon) mice. ***D***, Bar graphs represent the mean (±SEM) PSD-95 puncta densities in SR in the hippocampus and layers 1, 2/3, 5, and 6 in the PPC in unstressed P30 (blue), age-matched control (black), and stressed (red) mice. *$p < 0.05$, one-way ANOVA with Bonferroni's multiple-comparison test; ns, not significant.

induced neuronal activity (Dragunow and Faull, 1989; Senba et al., 1993), 60 min after stress exposure. Given the well documented effect of chronic stress on the hippocampus (Figueiredo et al., 2002), we performed the same staining in the CA1 region as a positive control. In RMS exposed mice, we found increased c-Fos immunoreactivity (Fig. 1*D*). Specifically, a single exposure to RMS increased the proportion of c-Fos$^+$ neurons approximately fivefold both in the PPC ($p < 0.01$, $n = 5$, one-way ANOVA corrected for multiple comparisons) and the hippocampus ($p < 0.001$, $n = 5$, one-way ANOVA corrected for multiple comparisons; Fig. 1*E*). One of the most important criticisms of experimental designs involving repeated stress exposure is that animals tend to get habituated to the stressors (Grissom and Bhatnagar, 2009). However, in the PPC, 10 d of RMS exposure resulted in the same proportion of c-Fos-labeled neurons as a single exposure ($p = 0.51$, $n = 6$ mice for 10 d and $n = 5$ mice for 1 d; one-way ANOVA corrected for multiple comparisons; Fig. 1*E*). Conversely, hippocampal c-Fos expression showed habituation effects indicated by reduced staining after 10 d of RMS ($p < 0.05$, $n = 5$, one-way ANOVA corrected for multiple comparisons; Fig. 1*E*), although it was still higher than control level ($p < 0.05$, $n = 5$, one-way ANOVA corrected for multiple comparisons; Fig. 1*E*). This is a critical result suggesting that neuronal activity in the PPC goes through marked changes as a result of RMS. When examining the laminar distribution of c-Fos$^+$ neurons, we found significantly fewer RMS-activated cells in layer 1 (average 4.7 ± 0.5 cells until 120 μm from the surface) then in other layers ($p < 0.001$, $n = 11$, one-way ANOVA with Bonferroni's correction; Fig. 1*F*). The distribution of labeled cells was even between layers 2/3 (12.1 ± 0.6 cell at 120–250 μm depth) and layer 5 (12.9 ± 0.3 cells at 250–600 μm depth, $p > 0.05$, $n = 11$, one-way ANOVA with Bonferroni's correction; Fig. 1*F*), but we found slightly fewer c-Fos-labeled neurons in layer 6 (10.0 ± 0.6 at 600 μm or deeper, $p < 0.001$, $n = 11$, one-way ANOVA with Bonferroni's correction; Fig. 1*F*) of the PPC.

RMS induces loss of excitatory synapses from the PPC

Repeated exposure to stress has been associated with a reduction of cortical thickness in humans (Eckart et al., 2011; Ansell et al., 2012) and a loss of neurons and excitatory synapses in rodent models, especially in the hippocampus and frontal cortical regions (Sousa et al., 2000; Radley et al., 2006). Using a fluorescent Nissl stain to label neurons (Fig. 2*A*,*B*), we found no evidence of neuron loss in either the PPC or the hippocampus of stressed mice when compared with controls (hippocampus, $p = 0.53$; PPC, $p = 0.82$, $n = 6$, Student's *t* test; data not shown). Cortical thickness also appeared to be unchanged by RMS (PPC thickness: 859 ± 17 vs 867 ± 26 μm, $p = 0.8$, $n = 6$, Student's *t* test, in control vs RMS, respectively). These data suggest that RMS does not induce macroscopic changes in the PPC.

To estimate synaptic connectivity of the PPC, we immunolabeled PSD-95 protein in brain slices prepared from age-matched control and RMS mice at the end of the 10 d stress regime. In the hippocampus and neocortex, PSD-95 has been shown in numerous studies to be a reliable marker of mature synapses, typically localized in dendritic spines and has been extensively used to detect stress-induced reduction in excitatory synapses (Cho et al., 1992; El-Husseini et al., 2000; Andres et al., 2013; Maras et al., 2014). As expected, PSD-95 immunolabeling resulted in a fine distribution of puncta in the cortex and hippocampus (Fig. 2*A*,*B*, cortex; hippocampal images not shown). We quantified PSD-95 puncta in PPC and hippocampal samples from age-matched control and RMS mice. Our results replicate previous findings of synapse number reduction in the hippocampus of stressed mice ($p = 0.0008$, $n = 6$, Student's *t* test; Fig. 2*C*). Furthermore, the number of PSD-95 puncta in the PPC was also significantly reduced by RMS (PPC: $p < 0.0001$, $n = 6$, Student's *t* test; Fig. 2*C*). We found that PSD-95 puncta density in P40 control animals was undistinguishable from P30 controls (PPC: $p = 0.89$, hippocampus: $p = 0.56$, $n = 6$, *t* test; Fig. 2*C*), suggesting that RMS causes the elimination of excitatory synapses rather than obstructing synapse formation during PPC development. Interestingly, we found that the cortical effect of adolescent RMS exposure persisted into adulthood: ~30 d after the last stress session, we still detected significant synapse loss in the PPC ($p = 0.008$, $n = 6$, *t* test; Fig. 2*C*), but not in the hippocampus ($p = 0.078$, $n = 6$, *t* test; Fig. 2*C*).

To better understand how this synapse loss might impact PPC connectivity, we decided to determine whether cortical layers were differentially affected. To this end, we randomly cropped 100 μm samples from layers 1, 2/3, 5, and 6 of the PPC images (Fig. 2*B*) and used similar samples of the stratum radiatum (SR) from hippocampal images as a positive control (no example shown). In accordance with previous literature, we saw significant synapse loss in the SR of the dorsal hippocampus in response to RMS ($p = 0.0039$, $n = 6$, Student's *t* test; Fig. 2*D*). In the PPC, RMS significantly reduced PSD-95 puncta numbers in layers 5 and 6, but not in more superficial layers (one-way ANOVA $p = 0.0015$, $F = 4.18$; Bonferroni's multiple-comparison test: L1, $p >$

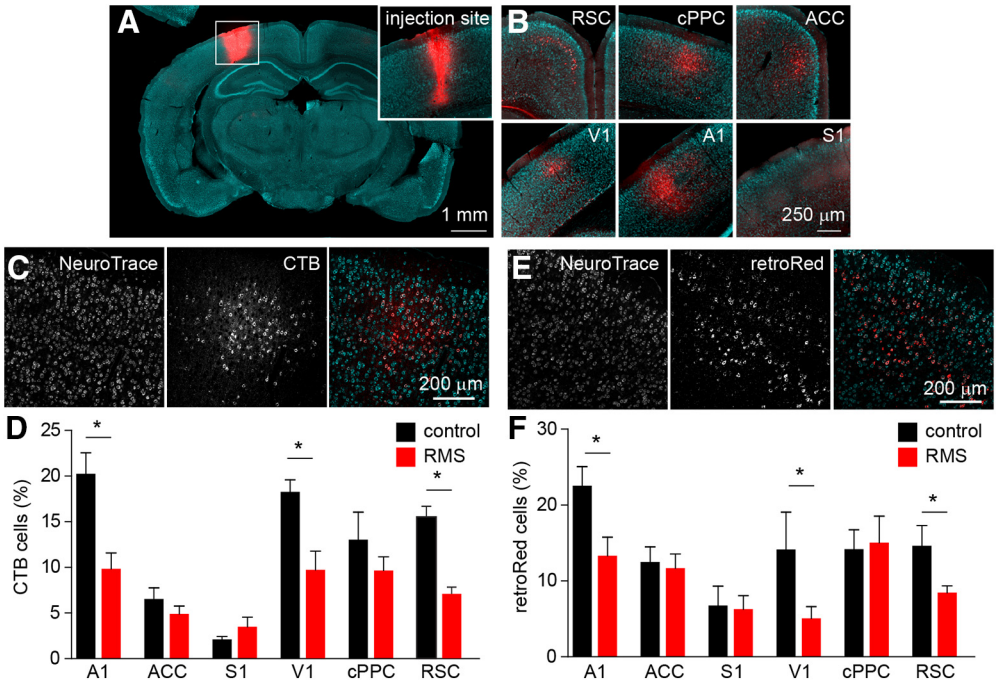

Figure 3. Circuit-specific loss of neuronal projections to the PPC following RMS. ***A***, representative image of the CTB-555 injection site. Inset, High-magnification image of the injection location. ***B***, Representative images of CTB-555-labeled projection cells in the RSC, the cPPC, the ACC, the V1, the A1, and the S1. ***C***, Representative confocal image of NeuTrace (cyan) CTB-555 (red)-labeled cells in the auditory cortex. ***D***, Bar graphs represent the mean (±SEM) proportion of CTB-555-labeled projection cells in cortical regions of control (black) and stressed (red) mice. ***E***, Representative confocal image of NeuTrace (cyan) red retrobead (red)-labeled cells in the auditory cortex. ***F***, Bar graphs represent the mean (±SEM) proportion of retrobead-labeled projection cells in different cortical regions of control (black) and stressed (red) mice. RSC, retrosplenial cortices. *$p < 0.05$, one-way ANOVA with Bonferroni's multiple-comparison test.

0.05; L2/3, $p > 0.05$; L5, $p < 0.05$; L6, $p < 0.01$; $n = 6$; Fig. 2*E*). We performed this laminar analysis on 30-d-old, unstressed mice as well and found that during the period of the experiment there is significant addition of synapses only in layer 1 ($p < 0.05$, one-way ANOVA with Bonferroni's correction for multiple comparisons; Fig. 2*D*). In deeper layers, we did not observe notable changes in synapse number from P30 to P40, suggesting that developmental changes are not likely to fully account for RMS-induced synapse loss.

Together, these data suggest that RMS does not affect parietal cortical thickness or neuron density but causes significant, layer-specific synapse loss from the PPC.

RMS causes region-specific loss of PPC projections

To identify the sources of cortical inputs affected by RMS, we labeled afferent neuronal populations projecting to the PPC using fluorescent retrograde tracing. We injected inactivated CTB conjugated to Alexa Fluor 555 dye (CTB-555) into the right PPC of age-matched control and stressed mice on day 4 of the RMS protocol. CTB-555 is taken up by axons in the PPC and is retrogradely transported to the somata of projection neurons (Fig. 3*A*; Dederen et al., 1994; Conte et al., 2009). Similarly to previous works (Wilber et al., 2015), we observed retrogradely labeled cell bodies in the retrosplenial cortex (RSC), the cPPC, the ACC, the V1, the A1, and, to a lesser extent, in the whisker region of the S1 (Fig. 3*B*). We used confocal microscopy to visualize these projection cells (Fig. 3*C*) and ask what proportion of cortical neurons is labeled in the above brain regions. If RMS had a uniform effect on the cortex, we would expect to see identical loss of projection neurons from all projection regions. On the contrary, we found significant projection cell loss from the A1, V1, and RSC regions (A1, $p < 0.001$; V1, $p < 0.01$; RSC, $p < 0.05$; one-way ANOVA, $p < 0.0001$, $F = 9.95$, $n = 7$, Bonferroni's multiple-comparison test; Fig. 3*D*). Intriguingly, the proportion of cells projecting to the PPC from the ACC, S1, and cPPC was indistinguishable between control and RMS animals ($p > 0.05$ in ACC, S1, and cPPC; one-way ANOVA, $n = 7$, Bonferroni's multiple-comparison test; Fig. 3*D*).

It is possible that the transport of CTB-555 is confounded by biological factors (e.g., CTB-555 retrograde transport may be activity dependent and thus affected by the bright light or the auditory stimulus during RMS). To ensure that our findings are independent of the tracing method, we repeated the above experiments with a different retrograde tracer: Lumafluor fluorescent latex microbeads (i.e., retrobeads; Fig. 3*E*). Our results with retrobeads were qualitatively indistinguishable from CTB-555 (A1, $p < 0.05$; V1, $p < 0.05$; RSC, $p < 0.05$; and $p > 0.05$ in ACC, S1, and cPPC; one-way ANOVA, $p < 0.0001$, $F = 5.62$, $n = 6$, Bonferroni's multiple-comparison test; Fig. 3*F*).

Our results were not driven by stress-induced neuron loss in the RMS group as we did not observe a difference in neuronal density between control and RMS animals in any of the cortical regions in either experiment (for CTB-555: $p = 0.76$, $F = 0.67$, $n = 7$, one-way ANOVA; for retrobeads: $p = 0.36$, $F = 1.12$, $n = 6$ one-way ANOVA, $p > 0.05$ for all comparisons in Bonferroni's *post hoc* multiple-comparison test). This result is in line with our observation above: 10 d of RMS does not appear to cause atrophy or other macroscopic changes in the cortex.

In summary, our data suggest that RMS causes region specific loss of long-range projections to the PPC.

RMS results in circuit-specific decrease of synaptic strength

Our data suggest that while anatomical signatures of auditory, visual, and retrosplenial inputs are eroded by RMS, frontal and contralateral PPC inputs are preserved. However, over the course of a 10 d period, plasticity mechanisms may counteract the loss of

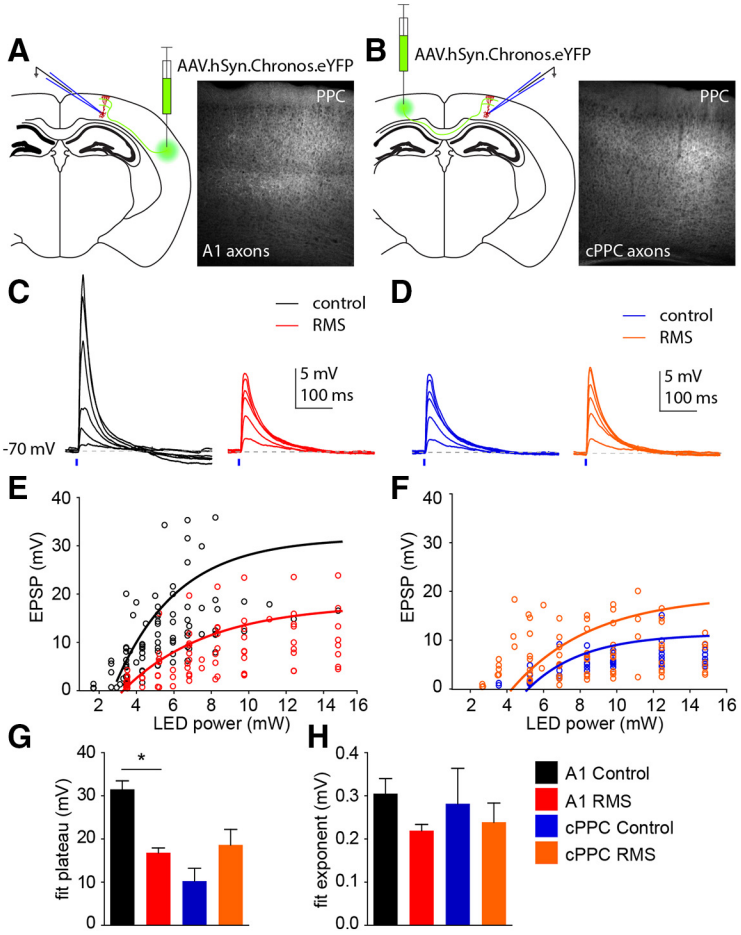

Figure 4. Circuit-specific reduction of synaptic strength by repeated, multimodal stress. ***A***, ***B***, Schematic illustrating the experiment (left) and wide-field image showing Chronos-expressing auditory (***A***) and cPPC (***B***) fibers in the recorded PPC hemisphere (right). ***C***, Example EPSP recordings evoked by stimulating auditory fibers in control (black) and stressed (red) animals. ***D***, Example EPSP recordings evoked by stimulating cPPC fibers in control (blue) and stressed (orange) animals. ***E***, Scatter plot showing the auditory EPSP magnitude–LED power relationship in control (black) and stressed (red) animals. Solid lines represent the reconstructed exponential fit from the mean of the calculated coefficients. ***F***, Scatter plot showing the cPPC EPSP magnitude–LED power relationship in control (blue) and stressed (orange) animals. Solid lines represent the reconstructed exponential fit from the mean of the calculated coefficients. ***G***, Bars represent the mean (±SEM) plateau from the exponential fit. ***H***, Bars represent the mean (±SEM) exponent from the exponential fit. *$p < 0.05$, Student's *t* test.

afferent inputs by increasing synaptic strength to preserve long-range connections. To test whether our anatomical findings translate to physiological differences, we sought to optogenetically drive PPC inputs to compare synaptic strength with or without stress. We expressed the excitatory channelrhodopsin variant Chronos in two regions that showed different sensitivity to RMS: A1 or in the cPPC (Fig. 4*A*,*B*). At the end of the RMS protocol, we made whole-cell current-clamp recordings from layer 5 pyramidal neurons in acute PPC slices prepared from control and stressed mice. To control for developmental stage and potential environmental differences, we recorded from an RMS and an age-matched control animal on the same day, using the same solutions and the same recording equipment. To test the strength of each afferent input, we measured the amplitude of EPSPs in response to increasingly powerful blue light pulses (Fig. 4*C*,*D*). To estimate the relationship between EPSP amplitude and LED power, we fitted the resulting data with an exponential function and compared the fit parameters (plateau and exponent) between control and RMS animals (Fig. 4*E*,*F*). We found that when stimulating auditory projections in control animals, EPSP amplitudes reached a higher plateau compared with animals subjected to RMS (31.48 ± 1.997 in control, $n = 4$ mice, compared with 16.81 ± 1.099 in RMS, $n = 4$ mice, $p = 0.0005$, *t* test; Fig. 4*E*,*G*). We also observed a trend toward faster rise of the EPSP amplitude/LED power relationship in controls (exponent = 0.31 ± 0.035 in control vs 0.22 ± 0.015 in RMS mice), although this trend was not significant ($p = 0.09$, *t* test; Fig. 4*H*). Conversely, RMS did not affect the EPSP–LED power relationship in cPPC afferents (plateau, $p = 0.13$; exponent, $p = 0.64$; $n = 4$ control and 5 RMS mice, Student's *t* test; Fig. 4*F*,*G*,*H*).

To test whether excitation and inhibition are differentially affected by RMS, we measured light-evoked EPSCs with membrane voltage clamped at −70 mV, and IPSCs with the membrane voltage clamped at 0 mV (Fig. 5*A*). We fitted light-evoked responses with an exponential function (Fig. 5*B*,*C*) and found that RMS exposure reduced the plateau of the fit for both EPSCs and IPSCs when activating A1 fibers in the PPC ($EPSC_{A1}$, $p = 0.043$; $IPSC_{A1}$, $p = 0.0077$; $n = 4$, *t* test; Fig. 5*D*,*E*). Neither EPSCs nor IPSCs evoked by cPPC stimulation were significantly affected by RMS ($EPSC_{cPPC}$, $p = 0.64$; $IPSC_{cPPC}$, $p = 0.9220$; $n = 5$, *t* test; Fig. 5*D*,*E*). We did not see a difference in the exponent value in any of our voltage-clamp experiments ($p > 0.1$ in all conditions; data not shown).

Altered EPSP magnitude may be driven by RMS-induced changes in intrinsic properties of the recorded neurons. To test this possibility, we measured membrane voltage responses to a series of negative and positive current injections in the cells recorded for Figure 4 (Fig. 6*A*,*B*). First, we found no difference in resting membrane potential of control and RMS cells (control: −75.66 ± 1.34 mV, $n = 14$; RMS: −72.9 ± 0.9 mV, $n = 12$; $p = 0.11$, Student's *t* test; Fig. 6*C*) or input resistance in response to negative current pulses (control: 136.9 ± 5.1 MΩ, $n = 14$; RMS: 141.7 ± 6.6 MΩ, $n = 12$; $p = 0.57$, Student's *t* test; Fig. 6*D*). However, in response to depolarizing current injections, we measured significantly higher input resistance in control cells (229.5 ± 14.36 MΩ in control, $n = 14$ vs 175.7 ± 14.01 in RMS; $n = 12$, $p = 0.014$, *t* test; Fig. 6*D*). Depolarizing current steps also evoked significantly more action potentials in mice subjected to MMS compared with controls ($p = 0.0001$, exposure to RMS explaining 3.63% of the total variance while the size of the current pulses explained a further 55.91% of the total variance in two-way ANOVA; Fig. 6*E*). We did not see a difference in action potential width ($p = 0.99$, two-way ANOVA; Fig. 6*F*), but RMS significantly decreased the distance between action potentials ($p < 0.0001$, 4.55% of total variance, two-way ANOVA; Fig. 6*G*) and action potent height ($p < 0.0001$, 7.51% of total variance, two-way ANOVA; Fig. 6*H*).

Altogether, these data are in strong agreement with our anatomical findings, suggesting that RMS causes circuit-specific deg-

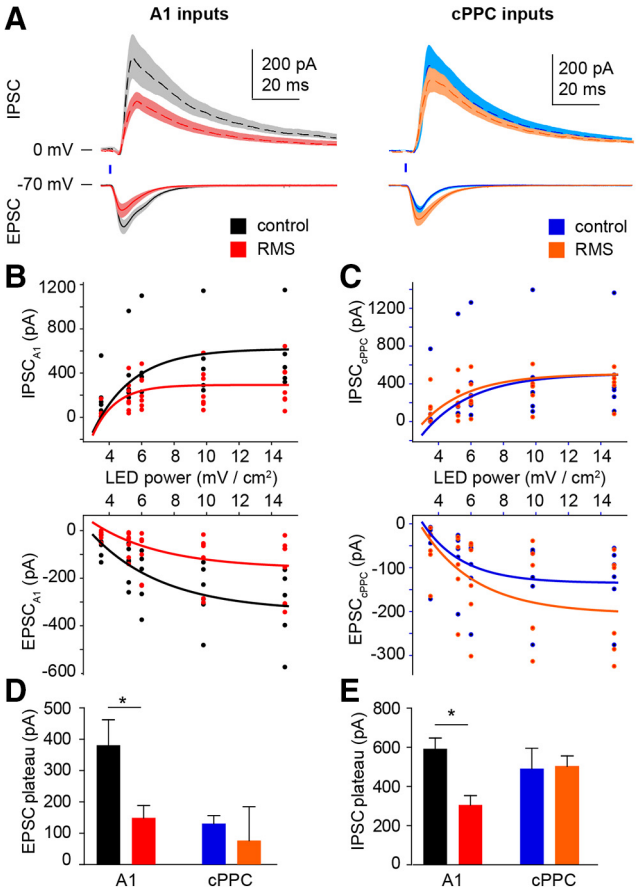

Figure 5. Circuit-specific effect of RMS on excitatory and inhibitory currents in the PPC. ***A***, Left, Average IPSC (dashed lines) and EPSC (solid lines) responses to optogenetic activation of A1 fibers in control (black) and RMS (red) mice. Right, Average IPSC (dashed lines) and EPSC (solid lines) responses to optogenetic activation of cPPC afferents in control (blue) and RMS (orange) mice. ***B***, ***C***, Population data showing increasing current amplitude in response to increasing LED power in control (black and blue) and stressed (red and orange) animals. Solid lines represent the mean exponential fit to the data. ***D***, Bars show the mean (±SEM) plateau of exponentials fitted to EPSCs. ***E***, Bars show mean (±SEM) plateau of exponential fitted to IPSCs. *$p < 0.05$, Student's *t* test.

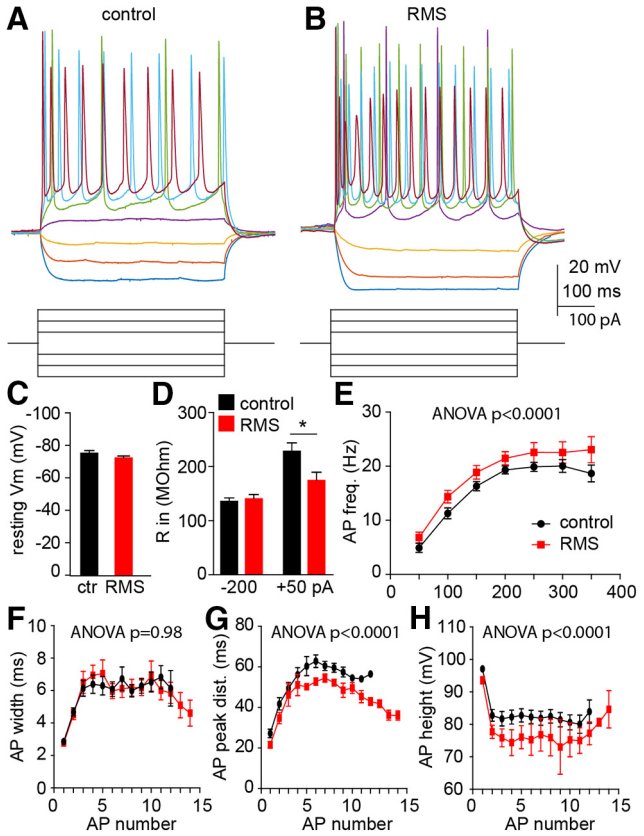

Figure 6. RMS increases the excitability of layer 5 pyramidal neurons in the PPC. ***A***, Example membrane potential responses to current pulses in a control mouse. ***B***, Example membrane potential responses to current pulses in a stressed mouse. ***C***, Comparison of resting membrane potential in control (black) and stressed (red) mice. ***D***, Comparison of input resistance in control (black) and stressed (red) mice. ***E–H***, Comparison of action potential firing frequency (***E***), action potential width (***F***), distance between action potential peaks (***G***), and action potential heights (***H***) in control and stressed mice. All bars represent the mean (±SEM); statistical comparisons: two-way ANOVA, *p* values are displayed above each graph. *$p < 0.05$, Student's *t*-test.

radation of long-range projections to the PPC while slightly increasing action potential firing in layer 5 pyramidal neurons.

Exposure to multiple concurrent stressors is necessary to influence the PPC circuit

To test whether the above observations are specific to RMS, we subjected separate cohorts of mice to 10 d of physical ROS (Fig. 7*A*) or bright light exposure (VIS) for 1 h/d. We found that ROS impaired weight gain ($p < 0.0001$, $n = 10$ control and 10 ROS mice, two-way ANOVA; Fig. 7*B*), similarly to RMS (Fig. 1*B*). However, spontaneous alternation in the Y-maze was not affected by either ROS ($p = 0.67$, $n = 9$ control and 9 ROS mice, *t* test; Fig. 7*C*) or VIS ($p = 0.63$, $n = 9$ control and 11 VIS mice, *t* test; Fig. 7*C*). The number of arm entries was also unaffected ($p = 0.54$ for ROS; and $p = 0.13$ for VIS; data not shown).

As expected based on the literature, ROS caused a reduction in PSD-95 puncta density in the hippocampus ($p < 0.01$, $n = 10$ control, $n = 6$ ROS, one-way ANOVA corrected for multiple comparisons; Fig. 7*D*) but not in the PPC ($p > 0.05$, $n = 11$ control, $n = 7$ ROS, one-way ANOVA corrected for multiple comparisons; Fig. 7*D*). Conversely, visual exposure did not affect synapse density in either structure ($p_{hip} > 0.05$, $p_{PPC} > 0.05$; $n = 4$ VIS mice, one-way ANOVA corrected for multiple comparisons; Fig. 7*D*).

We also examined the effect of ROS and VIS exposure on projection cell populations using the above-detailed CTB-555 retrograde labeling. The only significant difference we observed was a marked reduction in CTB-555-labeled neurons in the retrosplenial cortex of ROS mice ($p < 0.05$, $n = 9$ control, $n = 8$ ROS, $n = 7$ VIS, one-way ANOVA corrected for multiple comparisons; Fig. 7*E*).

These data are in line with the findings from other groups (Rogers and Kesner, 2006), suggesting that reduced spontaneous alternation performance, as we observed in RMS-exposed animals, is specifically due to PPC damage. Furthermore, these results indicate that the circuit-specific degradation of long-range projections to the PPC is not due to desensitization to the sensory stimuli presented during the stress sessions.

The role of V1 and the PPC in spontaneous alternation in the Y-maze

To directly test the role of the PPC in spontaneous alternations in the Y-maze, we implanted bilateral cannulas over the PPC (Fig. 8*A*,*B*). Following a 7 d recovery period, we injected the $GABA_A$ agonist (muscimol) or control vehicle (saline) into the cortex and measured spontaneous alternation in the Y-maze. On average, we found a 23% reduction in spontaneous alternations after musci-

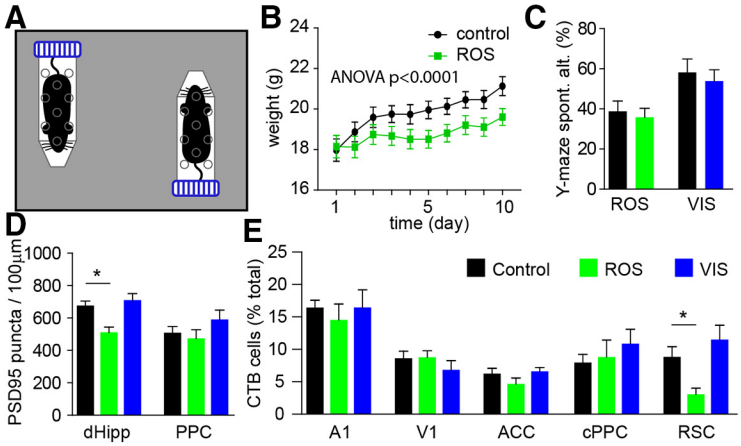

Figure 7. Single-modality stress paradigms have minimal effect on PPC. ***A***, Schematic of ROS. ***B***, Weight change of control (black) and stressed mice (green) during the 10 d exposure to ROS. Data points indicate the mean weight (±SEM) of mice on each day; figure shows result of two-way ANOVA test. ***C***, Bars represent spontaneous alternation percentage (±SEM) in control (black), ROS (green) and VIS (blue) exposed mice. ***D***, Bar graphs represent the mean (±SEM) PSD-95 puncta densities in the dorsal hippocampus (dHipp) and in the PPC in control (black), ROS (green), and VIS (blue) mice immediately after stress exposure. ***E***, Bar graphs represent the mean (±SEM) proportion of CTB-555-labeled projection cells in different cortical regions of control (black), ROS (green), and VIS (blue) mice. *$p < 0.05$, one-way ANOVA with Bonferroni's multiple-comparison test.

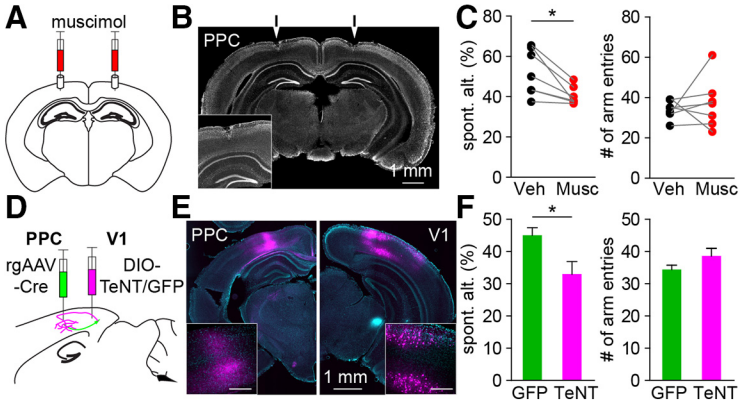

Figure 8. PPC activity and V1 long-range connectivity play a key role in navigating the Y-maze. ***A***, Schematic of cortical inhibition via muscimol. ***B***, Representative coronal section; arrows show the location of cannula implant. Inset, Higher-magnification image of the PPC. ***C***, Paired comparison of spontaneous alternation (left) and total number of arm entries (right) after saline (black) or muscimol (red) injection into the PPC. *$p < 0.05$, paired t test. ***D***, Schematic of the TeNT experiment. ***E***, Example images showing expression in V1 cell bodies (right) and afferent fibers in the PPC (left). Insets show magnified images of V1 and PPC. Scale bar, inset, 300 μm. ***F***, Bars represent mean (±SEM) spontaneous alternation percentage (left) and total number of arm entries (right) in GFP control (green) and TeNT-expressing (magenta) animals. *$p < 0.05$, paired t test.

mol when compared with vehicle injection ($p = 0.013$, $n = 7$, paired t test; Fig. 8*C*). We did not see a difference in the total number of arm entries ($p = 0.58$).

Finally, we were curious how RMS induced circuit-specific synapse loss related to reduced performance in the Y-maze. To answer this question, we bilaterally transduced the PPC with retrograde Cre-recombinase (rgAAV-hSyn-Cre-WPRE-hGH) to drive the expression of tetanus neurotoxin (AAV.DJ-CMV-DIO-eGFP-2A-TeNT) in PPC projection cells of the primary visual cortex (Fig. 8*D*,*E*). This strategy has been successfully used previously to suppress synaptic input from long-range projections in other brain regions (Xu et al., 2012; Xu and Südhof, 2013; Shang et al., 2018). We found that mice expressing TeNT (tetanus neurotoxin) in visual projections to the PPC performed 26% fewer spontaneous alternations compared with animals expressing GFP ($p = 0.017$, $n = 10$ animals in each group, unpaired t test; Fig. 8*F*).

These results confirm that altering the activity of the PPC impedes spontaneous alternation performance in the Y-maze similarly to RMS exposure. Furthermore, reducing V1 output to higher-order visual areas, including the PPC, also results in similarly diminished performance.

Discussion

In this study, we show that repeated exposure to multiple concurrent stressors (RMS) causes circuit-specific degradation of cortical inputs to the PPC and impairs spatial working memory. First, we show that RMS leads to disrupted neuronal activity- and layer-specific loss of excitatory synapses in the PPC. Using retrograde tracing, we found fewer PPC projecting neurons in the auditory, visual, and retrosplenial cortices of stressed animals but detected no change in the number of projection cells in the somatosensory, anterior cingulate, and contralateral PPC. We confirmed this reduction of sensory input to the PPC using electrophysiology. Finally, we demonstrated that the above effects are specific to multimodal stresses and lead to impaired behavioral performance.

In rodents, disrupted navigation has been a staple of stress-induced cognitive impairment. Although spatial tasks predominantly test hippocampal function, numerous studies pointed out that the PPC plays a subtle but critical role in these behaviors (Thomas and Weir, 1975; McNaughton et al., 1994; Spangler et al., 1994; Save and Poucet, 2000; Rogers and Kesner, 2006). Specifically, the PPC is linked to the working memory component of these spatial tasks (Kolb and Walkey, 1987; Save and Poucet, 2000; Whitlock et al., 2008). Our data demonstrate that reduced performance in Y-maze spontaneous alternation is specific to RMS and cannot be observed in mice subjected to restraint for an identical amount of time. This is despite a marked reduction in hippocampal PSD-95 labeling after restraint. The notion that RMS exerts this effect by specifically affecting the PPC is reinforced by our PPC inhibition experiments. Furthermore, ablating excitatory synapses of V1 neurons that project to the PPC caused similar behavioral effects to PPC inhibition and RMS. The goal of this manipulation was to approximate stress-induced, chronic synapse loss. The disadvantage of retrograde-Cre-driven TeNT expression is that it also removes the output of PPC-projecting V1 neurons to other cortical areas that are innervated by these cells. Thus, although it is not clear how many axon collaterals PPC-projecting V1 neurons send to non-PPC areas (Jarosiewicz et al., 2012; Glickfeld et al., 2013), the circuit specificity of this approach is weaker than acute techniques using local activation of DREADDs or opsins. Notably, restraint-induced impairment of visuospatial memory was previously observed in various mazes,

but only following exposure to much longer periods of restraint (Conrad et al., 1996, 2003; Ortiz et al., 2015). While this may suggest that the difference between RMS and other paradigms is the severity of stress exposure, multiple studies showed that blood corticosterone levels in response to RMS are indistinguishable from restraint or footshock stress (Magariños and McEwen, 1995; Maras et al., 2014; Lin et al., 2018). Whether the key difference is in the length of exposure, intensity, or the combination of stressors remains to be understood.

Other than navigation, the PPC has been associated with a wide range of executive functions including perceptual decision-making (Shadlen and Newsome, 2001; Harvey et al., 2012), working memory (Colby et al., 1996; Goard et al., 2016; Akrami et al., 2018), and attention (Buschman and Miller, 2007), many of which are thought to be vulnerable to stress (Dias-Ferreira et al., 2009; Liston et al., 2009; Friedman et al., 2017; Hart et al., 2017). To execute these functions, it is critical that the PPC integrates information from various brain regions (Johnson and Ferraina, 1996; Corwin and Reep, 1998; Reep and Corwin, 2009; Wilber et al., 2015; Meijer et al., 2019). Functional imaging (PET and fMRI) revealed altered metabolism in the parietal lobe of combat veterans (Bremner et al., 1999a), in women with a history of abuse (Bremner et al., 1999b, 2004; Lanius et al., 2002), and in subjects exposed to severe trauma (Piefke et al., 2007). Our data suggest that in mice, repeated exposure to multimodal stresses increased neuronal activity, measured via c-Fos expression, in the PPC. A previous study found similarly elevated levels of c-Fos in the PPC following social defeat stress (Lkhagvasuren et al., 2014). Disruption of parietal functional connectivity is a reoccurring observation among subjects exposed to chronic psychosocial stress or repeated traumatic events (Kolassa et al., 2007; Liston et al., 2009; Dunkley et al., 2015; Hart et al., 2017). In mice, we observed a marked decrease in the number of neurons projecting to the PPC in several cortical regions. While our results should not be equated to measurements in human functional imaging studies, they suggest that rodents may be a suitable model to study the effects of stress on regions other than the hippocampus or PFC.

Stress-induced synapse loss has been observed in a number of cortical regions, yet, layer-specific effects on synaptic markers is elusive. Csabai et al. (2018) found that stress-induced loss of type I (excitatory) synapses and myelinated axons is restricted to deeper layers of the infralimbic cortex. Our data extend these findings to the PPC, showing significant loss of PSD-95 staining only in layers 5 and 6. These observations have potential functional implications: the PPC is a region that receives both feedforward and feedback projections from other cortical regions (Wilber et al., 2015). Feedforward connections generally are constituted of sensory afferents that innervate deeper cortical layers while feedback inputs from higher-order brain areas are thought to target more superficial layers (Markov et al., 2014).

Although the identity of the synapses lost to stress is likely of importance, circuit-specific examinations are scarce. Stress-induced alteration of PFC–hippocampus local field potential correlations shows dorsoventral differences, indicating circuit-selective modulation (Lee et al., 2011). Furthermore, several cell populations have been distinguished in the PFC based on their reaction to repeated stress (Jackson and Moghaddam, 2006; Anderson et al., 2019). Indeed, stress-induced dendritic remodeling was shown to only affect select projection cells (Shansky et al., 2009). These studies suggest that the stress response may not be homogenous. Here we used two independent retrograde tracing methods, both indicating RMS-induced reduction in cells projecting to the PPC from auditory, visual, and retrosplenial cortices. Inputs from the contralateral PPC and from the anterior cingulate cortex appeared intact. We validated these results with electrophysiological measurements and confirmed that fewer projection cells correspond to weaker synaptic input to the PPC. Thus, we provide three independent lines of evidence suggesting that stress affects PPC inputs in a circuit-specific manner. Furthermore, by expressing tetanus neurotoxin (Xu et al., 2012; Xu and Südhof, 2013; Shang et al., 2018) in V1 neurons projecting to the PPC, we show that chronic ablation of V1 input to higher visual areas has similar behavioral effects to RMS. Future studies may use high-throughput methodology to present a more wholistic view of how input–output circuits of the PPC are affected by stress. Given the literature reviewed above it is likely that similar circuit specificity could be shown in the PFC.

Similar to our observations, repeated stress exposure has been shown to increase excitability in several brain regions, including the hippocampus, the PFC, and the amygdala (Lee et al., 2011; Kratzer et al., 2013; Hetzel and Rosenkranz, 2014; MacKenzie and Maguire, 2015; Czéh et al., 2018; Anderson et al., 2019). In the amygdala, increased action potential firing rate is due to stress-induced inhibition of calcium-activated K^+ channels (Rosenkranz et al., 2010; Hetzel and Rosenkranz, 2014). In other regions, studies reported reduced excitatory synaptic input (Urban and Valentino, 2017), altered inhibitory function (Ito et al., 2010; MacKenzie and Maguire, 2015; Czéh et al., 2018), or changes in voltage-gated ion channels (Kratzer et al., 2013). We found no apparent difference in resting membrane potential or the width of action potentials between control and stressed animals. However, in response to depolarizing current steps, we measured reduced input resistance after RMS. While this finding by itself cannot explain enhanced action potential firing, it suggests that RMS alters ion channel expression, recruitment, or conductivity that could influence firing threshold or the gain of the stimulus–response curve. Functional consequences of enhanced excitability may range from increased susceptibility to epileptic seizures (Dubé et al., 2015; MacKenzie and Maguire, 2015), hyperlocomotion (Ito et al., 2010) to a facilitation of certain memory formation processes (Yuen et al., 2009). Curiously, contextual fear conditioning and social isolation have been shown to reduce excitability in other neuronal cell types, indicating that the effects of stress on cellular properties are likely dependent on the type of the stressor and the examined cell type (Sargin et al., 2016; Soler-Cedeño et al., 2016).

In summary, we show that repeated exposure to multiple concurrent stressors exerts a robust effect on the PPC. These effects manifest in increased neuronal activity and significant loss of excitatory synapses, specifically from deeper cortical layers. We determined that synapse loss specifically impacts inputs from sensory and retrosplenial cortices, suggesting that the effects of stress are circuit specific. Functionally, RMS impairs spatial working memory performance in the Y-maze. Future experiments are needed to assess whether similarly specific effects can be observed in other brain areas and in human patients.

References

Akrami A, Kopec CD, Diamond ME, Brody CD (2018) Posterior parietal cortex represents sensory history and mediates its effects on behaviour. Nature 554:368–372.

Andersen RA, Cui H (2009) Intention, action planning, and decision making in parietal-frontal circuits. Neuron 63:568–583.

Andersen RA, Snyder LH, Bradley DC, Xing J (1997) Multimodal representation of space in the posterior parietal cortex and its use in planning movements. Annu Rev Neurosci 20:303–330.

Anderson EM, Gomez D, Caccamise A, McPhail D, Hearing M (2019) Chronic unpredictable stress promotes cell-specific plasticity in prefrontal cortex D1 and D2 pyramidal neurons. Neurobiol Stress 10:100152.

Andres AL, Regev L, Phi L, Seese RR, Chen Y, Gall CM, Baram TZ (2013) NMDA receptor activation and calpain contribute to disruption of dendritic spines by the stress neuropeptide CRH. J Neurosci 33:16945–16960.

Ansell EB, Rando K, Tuit K, Guarnaccia J, Sinha R (2012) Cumulative adversity and smaller gray matter volume in medial prefrontal, anterior cingulate, and insula regions. Biol Psychiatry 72:57–64.

Avital A, Richter-Levin G (2005) Exposure to juvenile stress exacerbates the behavioural consequences of exposure to stress in the adult rat. Int J Neuropsychopharmacol 8:163–173.

Bremner JD, Staib LH, Kaloupek D, Southwick SM, Soufer R, Charney DS (1999a) Neural correlates of exposure to traumatic pictures and sound in vietnam combat veterans with and without posttraumatic stress disorder: a positron emission tomography study. Biol Psychiatry 45:806–816.

Bremner JD, Narayan M, Staib LH, Southwick SM, McGlashan T, Charney DS (1999b) Neural correlates of memories of childhood sexual abuse in women with and without posttraumatic stress disorder. Am J Psychiatry 156:1787–1795.

Bremner JD, Vermetten E, Vythilingam M, Afzal N, Schmahl C, Elzinga B, Charney DS (2004) Neural correlates of the classic color and emotional stroop in women with abuse-related posttraumatic stress disorder. Biol Psychiatry 55:612–620.

Brodt S, Pöhlchen D, Flanagin VL, Glasauer S, Gais S, Schönauer M (2016) Rapid and independent memory formation in the parietal cortex. Proc Natl Acad Sci U S A 113:13251–13256.

Buschman TJ, Miller EK (2007) Top-down versus bottom-up control of attention in the prefrontal and posterior parietal cortices. Science 315:1860–1862.

Chen CC, Lu J, Yang R, Ding JB, Zuo Y (2018) Selective activation of parvalbumin interneurons prevents stress-induced synapse loss and perceptual defects. Mol Psychiatry 23:1614–1625.

Chen Y, Rex CS, Rice CJ, Dubé CM, Gall CM, Lynch G, Baram TZ (2010) Correlated memory defects and hippocampal dendritic spine loss after acute stress involve corticotropin-releasing hormone signaling. Proc Natl Acad Sci U S A 107:13123–13128.

Cho KO, Hunt CA, Kennedy MB (1992) The rat brain postsynaptic density fraction contains a homolog of the drosophila discs-large tumor suppressor protein. Neuron 9:929–942.

Colby CL, Duhamel JR, Goldberg ME (1996) Visual, presaccadic, and cognitive activation of single neurons in monkey lateral intraparietal area. J Neurophysiol 76:2841–2852.

Conrad CD, Galea LA, Kuroda Y, McEwen BS (1996) Chronic stress impairs rat spatial memory on the Y maze, and this effect is blocked by tianeptine pretreatment. Behav Neurosci 110:1321–1334.

Conrad CD, Grote KA, Hobbs RJ, Ferayorni A (2003) Sex differences in spatial and non-spatial Y-maze performance after chronic stress. Neurobiol Learn Mem 79:32–40.

Conte WL, Kamishina H, Reep RL (2009) The efficacy of the fluorescent conjugates of cholera toxin subunit B for multiple retrograde tract tracing in the central nervous system. Brain Struct Funct 213:367–373.

Corwin JV, Reep RL (1998) Rodent posterior parietal cortex as a component of a cortical network mediating directed spatial attention. Psychobiology 26:87–102.

Csabai D, Wiborg O, Czéh B (2018) Reduced synapse and axon numbers in the prefrontal cortex of rats subjected to a chronic stress model for depression. Front Cell Neurosci 12:24.

Czéh B, Vardya I, Varga Z, Febbraro F, Csabai D, Martis LS, Højgaard K, Henningsen K, Bouzinova EV, Miseta A, Jensen K, Wiborg O (2018) Long-term stress disrupts the structural and functional integrity of GABAergic neuronal networks in the medial prefrontal cortex of rats. Front Cell Neurosci 12:148.

Dagnino-Subiabre A (2013) Effects of chronic stress on the auditory system and fear learning: an evolutionary approach. Rev Neurosci 24:227–237.

Dederen PJ, Gribnau AA, Curfs MH (1994) Retrograde neuronal tracing with cholera toxin B subunit: comparison of three different visualization methods. Histochem J 26:856–862.

Dias-Ferreira E, Sousa JC, Melo I, Morgado P, Mesquita AR, Cerqueira JJ, Costa RM, Sousa N (2009) Chronic stress causes frontostriatal reorganization and affects decision-making. Science 325:621–625.

Dragunow M, Faull R (1989) The use of C-fos as a metabolic marker in neuronal pathway tracing. J Neurosci Methods 29:261–265.

Dubé CM, Molet J, Singh-Taylor A, Ivy A, Maras PM, Baram TZ (2015) Hyper-excitability and epilepsy generated by chronic early-life stress. Neurobiol Stress 2:10–19.

Dunkley BT, Sedge PA, Doesburg SM, Grodecki RJ, Jetly R, Shek PN, Taylor MJ, Pang EW (2015) Theta, mental flexibility, and post-traumatic stress disorder: connecting in the parietal cortex. PLoS One 10:e0123541.

Eckart C, Stoppel C, Kaufmann J, Tempelmann C, Hinrichs H, Elbert T, Heinze HJ, Kolassa IT (2011) Structural alterations in lateral prefrontal, parietal and posterior midline regions of men with chronic posttraumatic stress disorder. J Psychiatry Neurosci 36:176–186.

Eiland L, Romeo RD (2013) Stress and the developing adolescent brain. Neuroscience 249:162–171.

Eiland L, Ramroop J, Hill MN, Manley J, McEwen BS (2012) Chronic juvenile stress produces corticolimbic dendritic architectural remodeling and modulates emotional behavior in male and female rats. Psychoneuroendocrinology 37:39–47.

El-Husseini AE, Schnell E, Chetkovich DM, Nicoll RA, Bredt DS (2000) PSD-95 involvement in maturation of excitatory synapses. Science 290:1364–1368.

Figueiredo HF, Dolgas CM, Herman JP (2002) Stress activation of cortex and hippocampus is modulated by sex and stage of estrus. Endocrinology 143:2534–2540.

Friedman A, Homma D, Bloem B, Gibb LG, Amemori KI, Hu D, Delcasso S, Truong TF, Yang J, Hood AS, Mikofalvy KA, Beck DW, Nguyen N, Nelson ED, Toro Arana SE, Vorder Bruegge RH, Goosens KA, Graybiel AM (2017) Chronic stress alters striosome-circuit dynamics, leading to aberrant decision-making. Cell 171:1191–1205.e28.

Glickfeld LL, Andermann ML, Bonin V, Reid RC (2013) Cortico-cortical projections in mouse visual cortex are functionally target specific. Nat Neurosci 16:219–226.

Goard MJ, Pho GN, Woodson J, Sur M (2016) Distinct roles of visual, parietal, and frontal motor cortices in memory-guided sensorimotor decisions. Elife 5:e13764.

Gomes FV, Grace AA (2017) Adolescent stress as a driving factor for schizophrenia development—a basic science perspective. Schizophr Bull 43:486–489.

Grissom N, Bhatnagar S (2009) Habituation to repeated stress: get used to it. Neurobiol Learn Mem 92:215–224.

Hart H, Lim L, Mehta MA, Chatzieffraimidou A, Curtis C, Xu X, Breen G, Simmons A, Mirza K, Rubia K (2017) Reduced functional connectivity of fronto-parietal sustained attention networks in severe childhood abuse. PLoS One 12:e0188744.

Harvey CD, Coen P, Tank DW (2012) Choice-specific sequences in parietal cortex during a virtual-navigation decision task. Nature 484:62–68.

Hetzel A, Rosenkranz JA (2014) Distinct effects of repeated restraint stress on basolateral amygdala neuronal membrane properties in resilient adolescent and adult rats. Neuropsychopharmacology 39:2114–2130.

Ito H, Nagano M, Suzuki H, Murakoshi T (2010) Chronic stress enhances synaptic plasticity due to disinhibition in the anterior cingulate cortex and induces hyper-locomotion in mice. Neuropharmacology 58:746–757.

Jackson ME, Moghaddam B (2006) Distinct patterns of plasticity in prefrontal cortex neurons that encode slow and fast responses to stress. Eur J Neurosci 24:1702–1710.

Jarosiewicz B, Schummers J, Malik WQ, Brown EN, Sur M (2012) Functional biases in visual cortex neurons with identified projections to higher cortical targets. Curr Biol 22:269–277.

Johnson PB, Ferraina S (1996) Cortical networks for visual reaching: intrinsic frontal lobe connectivity. Eur J Neurosci 8:1358–1362.

Klapoetke NC, Murata Y, Kim SS, Pulver SR, Birdsey-Benson A, Cho YK, Morimoto TK, Chuong AS, Carpenter EJ, Tian Z, Wang J, Xie Y, Yan Z, Zhang Y, Chow BY, Surek B, Melkonian M, Jayaraman V, Constantine-Paton M, Wong GK, et al. (2014) Independent optical excitation of distinct neural populations. Nat Methods 11:338–346.

Kolassa IT, Wienbruch C, Neuner F, Schauer M, Ruf M, Odenwald M, Elbert T (2007) Altered oscillatory brain dynamics after repeated traumatic stress. BMC Psychiatry 7:56.

Kolb B, Walkey J (1987) Behavioural and anatomical studies of the posterior parietal cortex in the rat. Behav Brain Res 23:127–145.

Kratzer S, Mattusch C, Metzger MW, Dedic N, Noll-Hussong M, Kafitz KW, Eder M, Deussing JM, Holsboer F, Kochs E, Rammes G (2013) Activation of CRH receptor type 1 expressed on glutamatergic neurons increases excitability of CA1 pyramidal neurons by the modulation of voltage-gated ion channels. Front Cell Neurosci 7:91.

Lamprecht MR, Sabatini DM, Carpenter AE (2007) CellProfiler: free, versatile software for automated biological image analysis. Biotechniques 42:71–75.

Lanius RA, Williamson PC, Boksman K, Densmore M, Gupta M, Neufeld RW, Gati JS, Menon RS (2002) Brain activation during script-driven imagery induced dissociative responses in PTSD: a functional magnetic resonance imaging investigation. Biol Psychiatry 52:305–311.

Lee YA, Poirier P, Otani S, Goto Y (2011) Dorsal-ventral distinction of chronic stress-induced electrophysiological alterations in the rat medial prefrontal cortex. Neuroscience 183:108–120.

Lin X, Itoga CA, Taha S, Li MH, Chen R, Sami K, Berton F, Francesconi W, Xu X (2018) c-fos mapping of brain regions activated by multi-modal and electric foot shock stress. Neurobiol Stress 8:92–102.

Liston C, McEwen BS, Casey BJ (2009) Psychosocial stress reversibly disrupts prefrontal processing and attentional control. Proc Natl Acad Sci U S A 106:912–917.

Lkhagvasuren B, Oka T, Nakamura Y, Hayashi H, Sudo N, Nakamura K (2014) Distribution of fos-immunoreactive cells in rat forebrain and midbrain following social defeat stress and diazepam treatment. Neuroscience 272:34–57.

Luethi M, Meier B, Sandi C (2008) Stress effects on working memory, explicit memory, and implicit memory for neutral and emotional stimuli in healthy men. Front Behav Neurosci 2:5.

Luine V, Villegas M, Martinez C, McEwen BS (1994) Repeated stress causes reversible impairments of spatial memory performance. Brain Res 639: 167–170.

Lupien SJ, McEwen BS, Gunnar MR, Heim C (2009) Effects of stress throughout the lifespan on the brain, behaviour and cognition. Nat Rev Neurosci 10:434–445.

MacKenzie G, Maguire J (2015) Chronic stress shifts the GABA reversal potential in the hippocampus and increases seizure susceptibility. Epilepsy Res 109:13–27.

Magariños AM, McEwen BS (1995) Stress-induced atrophy of apical dendrites of hippocampal CA3c neurons: comparison of stressors. Neuroscience 69:83–88.

Maras PM, Molet J, Chen Y, Rice C, Ji SG, Solodkin A, Baram TZ (2014) Preferential loss of dorsal-hippocampus synapses underlies memory impairments provoked by short, multi-modal stress. Mol Psychiatry 19:745.

Markov NT, Vezoli J, Chameau P, Falchier A, Quilodran R, Huissoud C, Lamy C, Misery P, Giroud P, Ullman S, Barone P, Dehay C, Knoblauch K, Kennedy H (2014) Anatomy of hierarchy: feedforward and feedback pathways in macaque visual cortex. J Comp Neurol 522:225–259.

Mazzoni P, Bracewell RM, Barash S, Andersen RA (1996) Spatially tuned auditory responses in area LIP of macaques performing delayed memory saccades to acoustic targets. J Neurophysiol 75:1233–1241.

McNaughton BL, Mizumori SJ, Barnes CA, Leonard BJ, Marquis M, Green EJ (1994) Cortical representation of motion during unrestrained spatial navigation in the rat. Cereb Cortex 4:27–39.

McQuin C, Goodman A, Chernyshev V, Kamentsky L, Cimini BA, Karhohs KW, Doan M, Ding L, Rafelski SM, Thirstrup D, Wiegraebe W, Singh S, Becker T, Caicedo JC, Carpenter AE (2018) CellProfiler 3.0: Next-generation image processing for biology. PLoS Biol 16:e2005970.

Meijer GT, Mertens PEC, Pennartz CMA, Olcese U, Lansink CS (2019) The circuit architecture of cortical multisensory processing: distinct functions jointly operating within a common anatomical network. Prog Neurobiol 174:1–15.

Miedel CJ, Patton JM, Miedel AN, Miedel ES, Levenson JM (2017) Assessment of spontaneous alternation, novel object recognition and limb clasping in transgenic mouse models of amyloid-beta and tau neuropathology. J Vis Exp. Advance online publication. Retrieved May 28, 2017. doi: 10.3791/55523.

Mizoguchi K, Yuzurihara M, Ishige A, Sasaki H, Chui DH, Tabira T (2000) Chronic stress induces impairment of spatial working memory because of prefrontal dopaminergic dysfunction. J Neurosci 20:1568–1574.

Mohan H, de Haan R, Mansvelder HD, de Kock CPJ (2018) The posterior parietal cortex as integrative hub for whisker sensorimotor information. Neuroscience 368:240–245.

Noudoost B, Chang MH, Steinmetz NA, Moore T (2010) Top-down control of visual attention. Curr Opin Neurobiol 20:183–190.

Olcese U, Iurilli G, Medini P (2013) Cellular and synaptic architecture of multisensory integration in the mouse neocortex. Neuron 79:579–593.

Ortiz JB, Taylor SB, Hoffman AN, Campbell AN, Lucas LR, Conrad CD (2015) Sex-specific impairment and recovery of spatial learning following the end of chronic unpredictable restraint stress: potential relevance of limbic GAD. Behav Brain Res 282:176–184.

Piefke M, Pestinger M, Arin T, Kohl B, Kastrau F, Schnitker R, Vohn R, Weber J, Ohnhaus M, Erli HJ, Perlitz V, Paar O, Petzold ER, Flatten G (2007) The neurofunctional mechanisms of traumatic and non-traumatic memory in patients with acute PTSD following accident trauma. Neurocase 13:342–357.

Radley JJ, Rocher AB, Miller M, Janssen WG, Liston C, Hof PR, McEwen BS, Morrison JH (2006) Repeated stress induces dendritic spine loss in the rat medial prefrontal cortex. Cereb Cortex 16:313–320.

Reep RL, Corwin JV (2009) Posterior parietal cortex as part of a neural network for directed attention in rats. Neurobiol Learn Mem 91:104–113.

Reep RL, Chandler HC, King V, Corwin JV (1994) Rat posterior parietal cortex: topography of corticocortical and thalamic connections. Exp Brain Res 100:67–84.

Rogers JL, Kesner RP (2006) Lesions of the dorsal hippocampus or parietal cortex differentially affect spatial information processing. Behav Neurosci 120:852–860.

Romeo RD, Bellani R, Karatsoreos IN, Chhua N, Vernov M, Conrad CD, McEwen BS (2006) Stress history and pubertal development interact to shape hypothalamic-pituitary-adrenal axis plasticity. Endocrinology 147: 1664–1674.

Rosenkranz JA, Venheim ER, Padival M (2010) Chronic stress causes amygdala hyperexcitability in rodents. Biol Psychiatry 67:1128–1136.

Sargin D, Oliver DK, Lambe EK (2016) Chronic social isolation reduces 5-HT neuronal activity via upregulated SK3 calcium-activated potassium channels. Elife 5:e21416.

Save E, Poucet B (2000) Hippocampal-parietal cortical interactions in spatial cognition. Hippocampus 10:491–499.

Senba E, Matsunaga K, Tohyama M, Noguchi K (1993) Stress-induced c-fos expression in the rat brain: activation mechanism of sympathetic pathway. Brain Res Bull 31:329–344.

Shackman AJ, Maxwell JS, McMenamin BW, Greischar LL, Davidson RJ (2011) Stress potentiates early and attenuates late stages of visual processing. J Neurosci 31:1156–1161.

Shadlen MN, Newsome WT (2001) Neural basis of a perceptual decision in the parietal cortex (area LIP) of the rhesus monkey. J Neurophysiol 86: 1916–1936.

Shang C, Chen Z, Liu A, Li Y, Zhang J, Qu B, Yan F, Zhang Y, Liu W, Liu Z, Guo X, Li D, Wang Y, Cao P (2018) Divergent midbrain circuits orchestrate escape and freezing responses to looming stimuli in mice. Nat Commun 9:1232.

Shansky RM, Hamo C, Hof PR, McEwen BS, Morrison JH (2009) Stress-induced dendritic remodeling in the prefrontal cortex is circuit specific. Cereb Cortex 19:2479–2484.

Soares JM, Sampaio A, Ferreira LM, Santos NC, Marques F, Palha JA, Cerqueira JJ, Sousa N (2012) Stress-induced changes in human decision-making are reversible. Transl Psychiatry 2:e131.

Soler-Cedeño O, Cruz E, Criado-Marrero M, Porter JT (2016) Contextual fear conditioning depresses infralimbic excitability. Neurobiol Learn Mem 130:77–82.

Sousa N, Lukoyanov NV, Madeira MD, Almeida OF, Paula-Barbosa MM (2000) Reorganization of the morphology of hippocampal neurites and synapses after stress-induced damage correlates with behavioral improvement. Neuroscience 97:253–266.

Spangler EL, Heller B, Hengemihle J, Muth NJ, Jones BE, Garofalo P, Ingram DK (1994) Thrombosis of parietal, but not striate, cortex impairs acquisition of a 14-unit T-maze in the rat. Physiol Behav 56:95–101.

Thomas RK, Weir VK (1975) Effects of lesions in frontal or posterior association cortex of rats on maze iii. Physiol Psychol 3:210–214.

Ting JT, Daigle TL, Chen Q, Feng G (2014) Acute brain slice methods for

adult and aging animals: application of targeted patch clamp analysis and optogenetics. Methods Mol Biol 1183:221–242.

Urban KR, Valentino RJ (2017) Age- and sex-dependent impact of repeated social stress on intrinsic and synaptic excitability of the rat prefrontal cortex. Cereb Cortex 27:244–253.

Whitlock JR, Sutherland RJ, Witter MP, Moser MB, Moser EI (2008) Navigating from hippocampus to parietal cortex. Proc Natl Acad Sci U S A 105:14755–14762.

Wilber AA, Clark BJ, Demecha AJ, Mesina L, Vos JM, McNaughton BL (2015) Cortical connectivity maps reveal anatomically distinct areas in the parietal cortex of the rat. Front Neural Circuits 8:146.

Xu W, Südhof TC (2013) A neural circuit for memory specificity and generalization. Science 339:1290–1295.

Xu W, Morishita W, Buckmaster PS, Pang ZP, Malenka RC, Südhof TC (2012) Distinct neuronal coding schemes in memory revealed by selective erasure of fast synchronous synaptic transmission. Neuron 73:990–1001.

Yoshii T, Oishi N, Ikoma K, Nishimura I, Sakai Y, Matsuda K, Yamada S, Tanaka M, Kawata M, Narumoto J, Fukui K (2017) Brain atrophy in the visual cortex and thalamus induced by severe stress in animal model. Sci Rep 7:12731.

Yuen EY, Liu W, Karatsoreos IN, Feng J, McEwen BS, Yan Z (2009) Acute stress enhances glutamatergic transmission in prefrontal cortex and facilitates working memory. Proc Natl Acad Sci U S A 106:14075–14079.

Zhong L, Zhang Y, Duan CA, Deng J, Pan J, Xu NL (2019) Causal contributions of parietal cortex to perceptual decision-making during stimulus categorization. Nat Neurosci 22:963–973.